

High-temperature ferromagnetic semiconductor phase in rutile CrO₂ under biaxial compressive stress

Xiang-Bo Xiao¹ and Bang-Gui Liu^{1,2,*}

¹*Beijing National Laboratory for Condensed Matter Physics,*

Institute of Physics, Chinese Academy of Sciences, Beijing 100190, China

²*School of Physical Sciences, University of Chinese Academy of Sciences, Beijing 100190, China*

(Dated: December 14, 2024)

It is highly desirable to combine the full spin polarization of carriers with modern semiconductor technology for spintronic applications. For this purpose, one needs good crystalline ferromagnetic (or ferrimagnetic) semiconductors with high Curie temperatures. Rutile CrO₂ is a half-metallic spintronic material with Curie temperature 394 K and can have nearly-full spin polarization at room temperature. Here, we find through first-principles investigation that when a biaxial compressive stress is applied on rutile CrO₂, the density of states at the Fermi level decreases with the in-plane compressive strain and there is a phase transition to semiconductor phase at the strain of -6.1%, but its ferromagnetic Curie temperature remains almost independent of the strain. Further analysis shows that this half-metal-semiconductor transition is induced by the special stress-driven distortion of the oxygen octahedron of Cr in the rutile structure. This biaxial stress can be realized by applying biaxial pressure or growing the rutile CrO₂ epitaxially on appropriate substrates. These results should be useful for realizing full spin polarization of controllable carriers as one uses in modern semiconductor technology.

I. INTRODUCTION

It is always of much interest to search for high-performance spintronic materials¹⁻⁴. Full spin polarization can be realized in half-metallic materials^{4,5} such as rutile CrO₂⁶⁻⁹, because one of the two spin channels is metallic and the other has a semiconductor gap. For rutile CrO₂, ferromagnetic Curie temperature can reach to 394 K and great effort has been made to achieve high-quality materials for full spin polarization¹⁰⁻¹⁶. It is also interesting to seek half-metallic materials based on semiconductors^{4,17-22}. Furthermore, one naturally hope to combine the full polarization with modern semiconductor technology. For this purpose, one needs crystalline ferromagnetic (or ferrimagnetic) semiconductors with high Curie temperatures and then choose appropriate dopants for controllable carriers. In this direction, many good materials have been found, and among them, perovskite Ca₂CrReO₆, Ca₂FeReO₆, and Sr₂CrOsO₆ are ferrimagnetic semiconductors, and their Curie temperatures are 360 K, 522 K, and 725 K, respectively²³⁻²⁶. Along this line, it is hopeful to realize full (or at least nearly full) spin polarization for controllable concentrations of high-mobility carriers beyond room temperature.

Here, we present strain-induced high-temperature ferromagnetic semiconductor phase in rutile CrO₂ in terms of first-principles calculation. Biaxial compressive stress is applied to rutile CrO₂ to make the in-plane lattice constant a reduce by up to -10%, with the other lattice constant determined by stress equilibrium. The stress makes the horizontal bonds (Cr-O and O-O) compress linearly, the oblique bonds (Cr-O) remain almost unchanged, and the side bond-angle (between two oblique bonds) decrease linearly. With the stress increasing, the density of states at the Fermi level decreases substantially, and finally the rutile CrO₂ becomes a semiconduc-

tor when a is compressed by 6.1%. It is very interesting that for all the compression, the inter-spin exchange energies remain almost unchanged and then the Curie transition temperature still remains near 400 K. Our analysis indicates that this half-metal-semiconductor transition is driven by the special distortion of the oxygen octahedron of Cr in the rutile structure. This could open a door to achieve crystalline ferromagnetic semiconductors with high Curie temperatures. More detailed results will be presented in the following.

II. COMPUTATIONAL DETAILS

Our density-functional-theory calculations are done with the Vienna package WIEN2K²⁷, which is a full-potential augmented plane wave plus local orbital program within the density functional theory^{28,29}. For total energy calculation of rutile CrO₂, we take the generalized-gradient approximation (GGA)³⁰ for the exchange-correlation potential. The scalar approximation is taken for the relativistic effects of valence states. For improving the electronic structure calculations, we use modified Becke-Johnson (mBJ)³¹ exchange potential plus GGA correlation potential for the exchange-correlation potential. The muffin-tin radii (R_{mt}) of Cr and O atom are optimized to achieve high accuracy. We use 3000 k points in the Brillouin zone and set $R_{mt} \times K_{max}$ to 7.0, and in addition, we make angular momentum expansion up to $l_{max}=10$ in the muffin tins. When the integrated absolute value of the charge difference per formula unit, $\int |\rho_n - \rho_{n-1}| dr$, between the input charge density $[\rho_{n-1}(r)]$ and the output charge density $[\rho_n(r)]$ is less than 0.0001 $|e|$ where e is the electron charge, the self-consistent calculation will be considered to be converged. The spin-orbit coupling is also taken

into account to investigate the spin polarization at the Fermi level.

III. RESULTS AND DISCUSSION

A. Strain-dependent structure parameters

Rutile CrO_2 assumes a tetrahedral structure with the space group $P4_2/mnm$ (#136)⁶⁻⁹, as shown in Fig. 1. There are two formula units in the unit cell. Two chromium atoms are located at $(0,0,0)$ and $(\frac{1}{2}, \frac{1}{2}, \frac{1}{2})$ in the internal coordinates, and four oxygen atoms at $(u, u, 0)$, $(1-u, 1-u, 0)$, $(\frac{1}{2}+u, \frac{1}{2}-u, \frac{1}{2})$, and $(\frac{1}{2}-u, \frac{1}{2}+u, \frac{1}{2})$, respectively, where u (≤ 1) is a dimensionless internal coordinate parameter. We have fully optimized the lattice constants (a and c) and the internal coordinate parameter u by using GGA. The resulting equilibrium structural parameters (a_0 , c_0 , and u_0) are equivalent to 4.4507Å, 2.9317Å, and 0.304, respectively. The electronic structure is half-metallic, which is consistent with previous DFT calculated results and experimental observations.

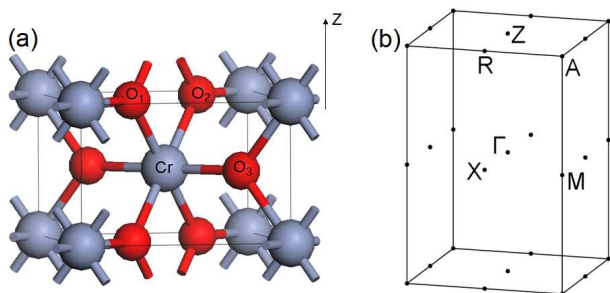


FIG. 1. (Color online) The crystal structure (a) and the Brillouin zone (b) of rutile CrO_2 .

In order to manipulate the electronic structure, we can apply a biaxial stress to the rutile CrO_2 . Such stress can be realized by applying pressure along the x and y axes or growing the rutile CrO_2 as epitaxial [001] thin films on some suitable substrates. Since tensile stress has limited effect on the electronic states of the CrO_2 near the Fermi level, we will concentrate on compressive stress within the x-y plane. We use dimensionless parameter $\Delta a/a_0 = (a - a_0)/a_0$ to describe the strain in the x and y axes, where a is the lattice constant in the x-y plane of the strained rutile CrO_2 . $\Delta a/a_0 = 0$ corresponds to the equilibrium lattice. For a given in-plane lattice constant $a < a_0$, we make a full structural optimization to determine the other lattice constant c and the internal parameter u . The total energy of the strained CrO_2 is calculated with the optimized strained crystal structure. We have done a series of optimization with $0 > \Delta a/a_0 \geq -10\%$. The structural parameters (a , c , and u) and total energy (E) values are summarized in Table I.

As the compressive strain, $-\Delta a/a_0$, increases (a decreases), c increases, and the internal parameter u increases slightly. The opposite trend of a and c reflects

TABLE I. Optimized structural parameters (c and u) and total energy per formula unit (E) calculated with GGA of rutile CrO_2 ferromagnetic phase for different in-plane lattice constant a and its relative change $\Delta a/a_0$. The semiconductor gap (G_s) values are calculated with mBJ.

$\Delta a/a_0$ (%)	a (Å)	c (Å)	u	E (eV)	G_s (eV)
0	4.4507	2.9317	0.304	0	-
-3.0	4.3172	3.0000	0.305	0.130	-
-5.0	4.2282	3.0456	0.306	0.386	-
-5.5	4.2059	3.0624	0.306	0.474	-
-5.8	4.1926	3.0708	0.306	0.530	-
-6.0	4.1837	3.0792	0.306	0.571	-
-6.2	4.1748	3.0877	0.306	0.617	0.01
-6.5	4.1614	3.0962	0.306	0.680	0.02
-7.0	4.1392	3.1182	0.307	0.796	0.10
-8.0	4.0946	3.1245	0.308	1.064	0.14
-9.0	4.0501	3.1679	0.309	1.384	0.30
-10.0	4.0056	3.1910	0.310	1.748	0.41

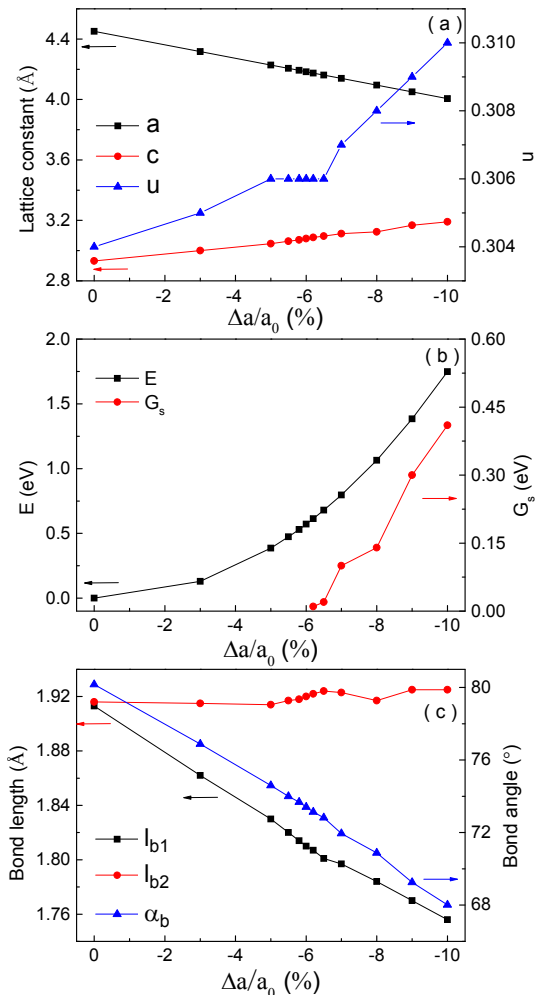


FIG. 2. (Color online) The $\Delta a/a_0$ dependence of structural parameters (a , c , u) (a), total energy (E) and semiconductor gap G_s (b), and bond parameters (l_{b1} , l_{b2} , α_b) (c).

the trend that with stress applied, the volume tries to remain unchanged. Because c becomes large with the biaxial compression increasing, there is actually a tensile strain in the z axis. The stronger the compression is, the larger the energy E becomes, which is expected because the strain drive the CrO_2 to deviate from the equilibrium structure. More importantly, there is a phase transition from the half-metallic phase to a semiconductor when the compression ratio of a reaches to -6.1% . We visualize these trends of a , c , u , E , and G_s in Fig. 2 by plotting them as functions of the compression ratio, $\Delta a/a_0$. The behavior of E is regular, as expected. It is clear that the lattice constants change almost linearly with $\Delta a/a_0$ decreasing, the parameter u has little change near the transition point, and the semiconductor gap grows fast after being created at the transition point.

It is vital to check the stability of ferromagnetic order and Currier temperature against the biaxial compression. Because the biaxial compression enhances the ferromagnetic exchange in the x - y plane and maybe weakens the ferromagnetic exchange in the z direction, we have constructed antiferromagnetic order along the z direction and compared their total energies with the ferromagnetic rutile CrO_2 for $\Delta a/a_0 = 0, -3.0, -5.0, -6.0, -7.0, -8.0, -9.0$, and -10.0% , respectively. For the eight $\Delta a/a_0$ values, our calculated results show that the ferromagnetic rutile CrO_2 is lower than the antiferromagnetic configuration by 0.320, 0.346, 0.352, 0.354, 0.354, 0.348, 0.338, and 0.328 eV per formula unit, respectively. Therefore, the ferromagnetic order is stable against spin fluctuation and when the biaxial compression is applied, the Currier temperature should remain approximately the same as that of the equilibrium structure^{4,14-16}.

TABLE II. The lattice constant ratios (c/a), bond angles (α_b), and bond lengths (l_{b1} and l_{b2}) for different $\Delta a/a_0$ values.

$\Delta a/a_0$ (%)	c/a	α_b ($^\circ$)	l_{b1} (\AA)	l_{b2} (\AA)
0	0.6587	80.17	1.913	1.916
-3.0	0.6949	76.88	1.862	1.915
-5.0	0.7203	74.60	1.830	1.914
-5.5	0.7281	74.00	1.820	1.917
-5.8	0.7324	73.68	1.814	1.918
-6.0	0.7360	73.41	1.810	1.920
-6.2	0.7396	73.14	1.807	1.922
-6.5	0.7440	72.82	1.801	1.924
-7.0	0.7520	71.95	1.797	1.923
-8.0	0.7631	70.88	1.784	1.917
-9.0	0.7822	69.26	1.770	1.925
-10.0	0.7966	68.01	1.756	1.925

In order to find out the relationship between the electronic properties and the crystal structure, we also present in Table 2 the ratio c/a , the bond angle (α_b), and bond lengths (l_{b1} for Cr-O3 bond and l_{b2} for Cr-O2) of rutile CrO_2 for different $\Delta a/a_0$ values. Here, α_b denotes the O1-Cr-O2 bond angle, and l_{b1} and l_{b2} indicate the lengths of the Cr-O3 and Cr-O2 bonds, respectively. It should be noted that the Cr-O3 bond is

always perpendicular to the Cr-O1 and Cr-O2 bonds. At the same time, we plot in Fig. 2(c) the bond lengths and the bond angle as functions of different compression ratio of lattice constant a . It is clear that the bond angle and the bond length l_{b1} almost linearly decrease with $\Delta a/a_0$ changing from 0 to -10% , whereas the other bond length l_{b2} changes only a little. Our analysis shows that the almost-linear decrease of the Cr-O3 bond length is caused directly by the decrease of the lattice constant a , and the Cr-O2 bond length remains almost unchanged because the decrease of the bond angle α_b compensates the opposite changes of a and c .

B. Electronic structures and phase transition

We present in Fig. 3 the total and partial density of states calculated with mBJ for three $\Delta a/a_0$ values: 0, -6.0% , and -8.0% . For the equilibrium structure (Fig. 3a), we found through our mBJ calculations that there is a big gap in the minority spin channel around the Fermi level, but the band structure is metallic in the majority spin channel, which is consistent with the fact that rutile CrO_2 is a half-metal⁷. As we decrease the lattice constant a , the total density of states at the Fermi level reduces in the majority spin channel, as shown in Fig. 3b for $\Delta a/a_0 = -6.0\%$. When the lattice constant a is compressed by more than 8% , it is clear that the total density of states at the Fermi level becomes zero, as shown in Fig. 3c for $\Delta a/a_0 = -8.0\%$, and consequently we obtain a ferromagnetic semiconductor phase. These electronic structures show an electronic phase transition from half-metal to ferromagnetic semiconductor for the rutile CrO_2 material. The low DOS near the Fermi level reflects that the O p electrons are distributed mainly out of the O muffin tin, which is consistent with the large DOS contribution from the interstitial region.

In order to investigate the electronic properties of these systems in detail, we have also calculated the orbit-resolved density of states. The detailed orbit-resolved density of states in the vicinity of the Fermi level are shown in Fig. 4. For the equilibrium structure, Cr d_{xy} and d_{yz} orbitals make the Cr 3d states near the Fermi level in the majority spin channel, as shown in Fig. 4a. As for the O 2p states, the p_x orbital is dominant near the Fermi level, as shown in Fig. 4b. As the lattice constant a decreases, the Cr d_{xy} orbital gradually disappear from below the Fermi level and only Cr d_{yz} remains there. As shown in Fig. 4c, at $\Delta a/a_0 = -6.0\%$, the Cr d_{xy} orbital is above the Fermi level and Cr d_{yz} remains below the Fermi level. At $\Delta a/a_0 = -6.1\%$, there is gap open at the Fermi level which divides the Cr d_{xy} and d_{yz} states, and the gap grows when the a is compressed further, reaching to 0.14 eV at $\Delta a/a_0 = -8.0\%$, as shown in Fig. 4e. In the meantime, there is only O p_x orbital near the Fermi level, as shown in Fig. 4d and 4f. These imply that when $\Delta a/a_0$ is beyond -6.1% , the valence band top is occupied by Cr d_{yz} and O p_x orbitals only, and the conduction

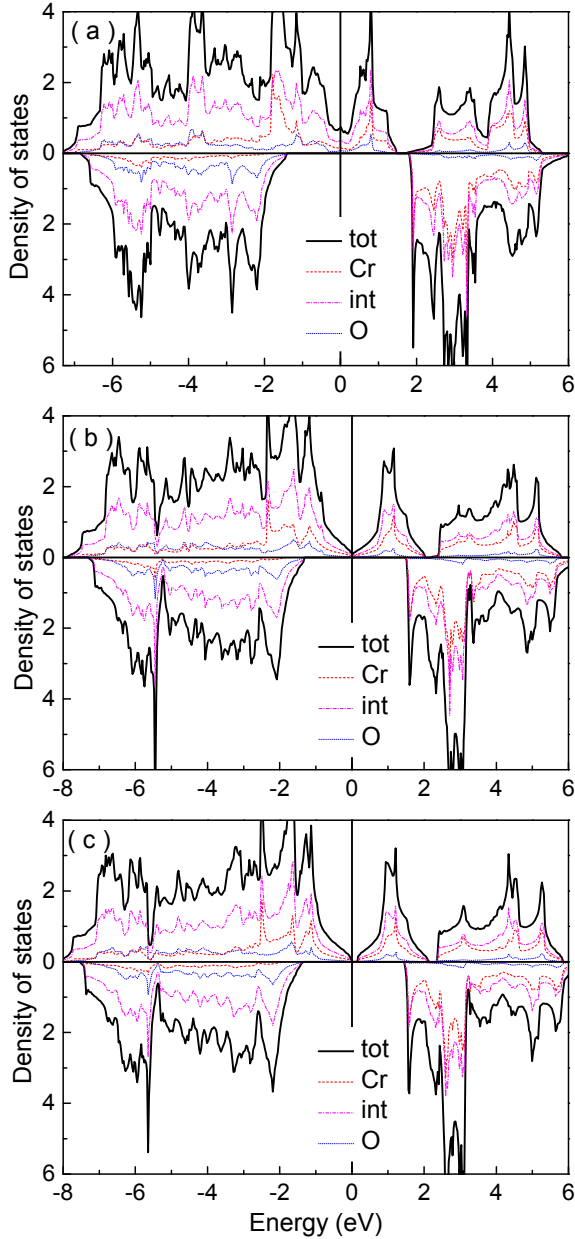


FIG. 3. (Color online) Spin-resolved total and partial density of states of rutile CrO_2 for (a) the calculated equilibrium structural parameters ($a = 4.4507 \text{ \AA}$, $c = 2.9317 \text{ \AA}$, $u = 0.304$); (b) the structure with a compressed by 6% ($a = 4.1837 \text{ \AA}$, $c = 3.0792 \text{ \AA}$, $u = 0.306$); and (c) the structure with a compressed by 8% ($a = 4.0946 \text{ \AA}$, $c = 3.1245 \text{ \AA}$, $u = 0.308$).

band bottom by Cr d_{xy} and o p_x only.

We present in Fig. 5 the band structures of strained rutile CrO_2 for three $\Delta a/a_0$ values: 0, -6.0%, and -8.0%. It is clear that without any strain, the rutile CrO_2 is a typical half-metal with a large gap in the minority-spin channel, as show in Figs. 5a and 5b. As we decrease the lattice constant a , the bands near the Fermi level tend to move away from the Fermi level in the majority-spin channel,

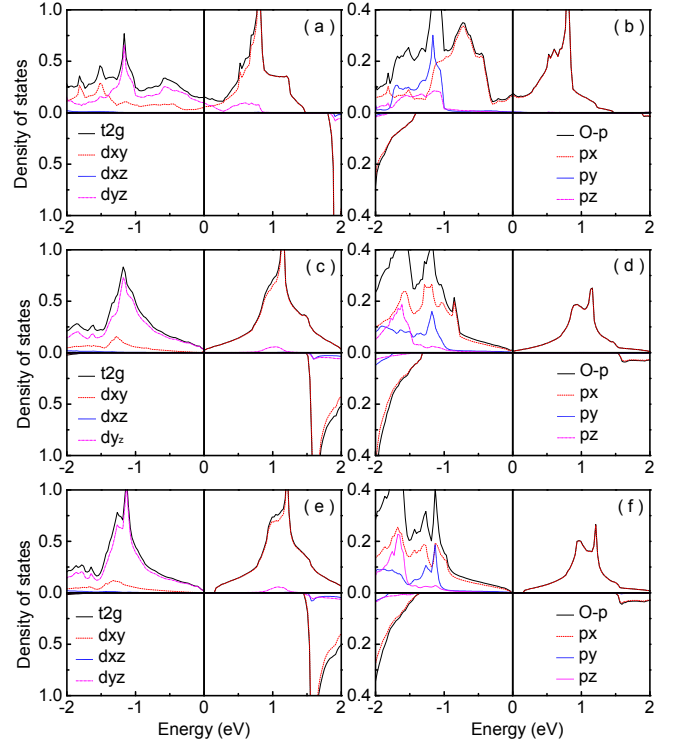


FIG. 4. (Color online) Orbital-resolved partial density of states of Cr-t2g and O-p (a,b) for the calculated equilibrium structural parameters ($a = 4.4507 \text{ \AA}$, $c = 2.9317 \text{ \AA}$, $u = 0.304$); (c,d) for the structure with a compressed by 6% ($a = 4.1837 \text{ \AA}$, $c = 3.0792 \text{ \AA}$, $u = 0.306$); and (e,f) for the structure with a compressed by 8% ($a = 4.0946 \text{ \AA}$, $c = 3.1245 \text{ \AA}$, $u = 0.308$), respectively.

with the gap remaining still wide in the minority-spin channel. The transition happens at $\Delta a/a_0 = -6.1\%$, from which on there is a gap open at the Fermi level in the majority-spin channel. The conduction band minimum is at the Γ point in the Brillouin zone, and the valence band maximum at the Z point, which implies that the strained rutile CrO_2 is an indirect gap semiconductor. The majority-spin gap is approximately at the middle of the minority-spin gap. We can see a special feature that when the majority-spin gap is open, there are two empty majority-spin bands between the Fermi level and +2 eV. Combining with the DOS in the same energy window, we can conclude that they originate mainly from O p_x and Cr d_{xy} orbitals. In contrast, the filled bands between -0.8 eV and the Fermi level originate mainly from the O p_x and Cr d_{yz} orbitals.

C. Further discussions

Furthermore, we show the strain dependence of the oxygen octahedron and the key bond lengths and bond angles in rutile CrO_2 . In Fig. 6 we present the strain dependence of the bond length (l_{b1}) between Cr1 and O6

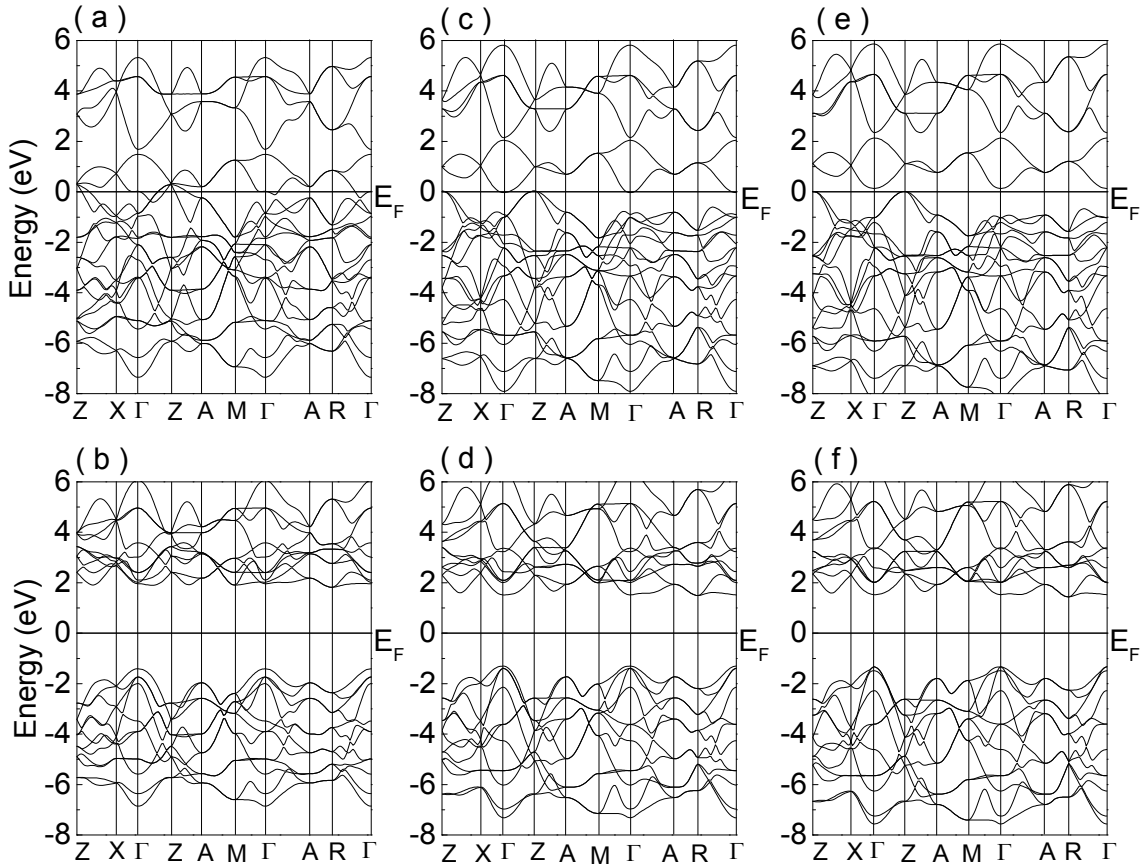


FIG. 5. Spin-polarized band structures of rutile CrO_2 (a,b) for the calculated equilibrium structural parameters ($a = 4.4507\text{\AA}$, $c = 2.9317\text{\AA}$, $u = 0.304$); (c,d) for the structure with a compressed by 6% ($a = 4.1837\text{\AA}$, $c = 3.0792\text{\AA}$, $u = 0.306$); and (e,f) for the structure with a compressed by 8% ($a = 4.0946\text{\AA}$, $c = 3.1245\text{\AA}$, $u = 0.308$), respectively. The upper row presents the majority-spin band structure, and the lower row the minority-spin one.

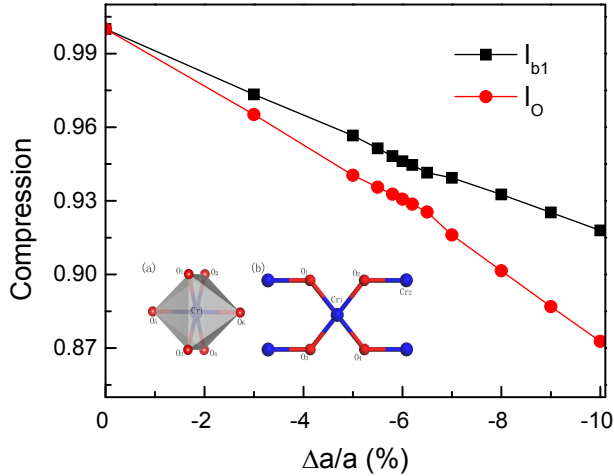


FIG. 6. The strain-dependent compression of the horizontal bond (l_{b1}) and the O-O distance (l_O). Inset: The oxygen octahedron (a) and the key bond lengths and bond angles (b).

(or between O2 and Cr2) and the O-O bond length (l_O)

that can be defined as the distance between O1 and O2. As described in the insert of Fig. 6, the angle α_b describes the bond angle O1-Cr1-O2 and l_{b2} is the bond length between Cr1 and O1. We can see in Fig. 2 and Table II that when the biaxial compressive stress is applied, both l_{b1} and l_{b2} decrease linearly, but l_{b2} remains almost unchanged. The O-O bond length l_O also decreases with the compressive stress increasing. It is clear that the O-O bond length l_O is compressed more easily than the horizontal bond length l_{b1} . This implies that it is more easy to compress the bond angle α_b than to compress the horizontal length l_{b1} . These changes of the bond lengths and angles mean that the oxygen octahedron is distorted.

We can realize such compression by growing rutile CrO_2 on good oxide substrates such as CoO, MgO, NiO, and BaSnO_3 ^{32,33}. For these four substrates, the lattice mismatch is between -3.4% and -7%, and the stress is between 15 and 32 GPa. Accordingly, the first three heterostructures (CrO_2/CoO , CrO_2/MgO , CrO_2/NiO) should still be half-metallic, and the heterostructure $\text{CrO}_2/\text{BaSnO}_3$ should be semiconductive. Because the Curie temperature for such strain values should remain

almost the same as that of equilibrium strain-free structure, we can manipulate the transport properties of rutile CrO_2 by growing it on different substrates.

IV. CONCLUSION

We have investigated the structural, magnetic, electronic properties of rutile CrO_2 under biaxial compressive stress through first-principles calculation. mBJ exchange potential is used to improve the description of the electronic structure. The biaxial compressive stress makes the in-plane lattice constant a decrease and the out-of-plane c increase. Correspondingly, the two horizontal Cr-O and O-O bond-lengths and the side O-Cr-O bond-angle decrease linearly, but the oblique bond-lengths remain almost unchanged. Our total energy comparison shows that the Curie temperature of the rutile CrO_2 under the stress remains almost the same as that (near 400 K) without any stress. As for the electronic structure, the density of states decreases with the a becoming small and there is a half-metal-semiconductor transition at $\Delta a/a_0 = -6.1\%$. Full spin polarization can be re-

alized for controllable concentration of carriers by usual gating or doping in modern semiconductor technology. Our further analysis shows that this semiconducting ferromagnetic phase is driven by the biaxial-stress-induced distortion of the oxygen octahedron of Cr in the rutile structure. This biaxial compression can be realized by applying biaxial pressure or growing rutile CrO_2 epitaxially on appropriate substrates. Therefore, these could pave a road to achieve good ferromagnetic semiconductors for spintronic applications.

ACKNOWLEDGMENTS

This work is supported by the Nature Science Foundation of China (Grant No. 11574366), by the Strategic Priority Research Program of the Chinese Academy of Sciences (Grant No. XDB07000000), and by the Department of Science and Technology of China (Grant No. 2016YFA0300701). All the numerical calculations were performed in the Milky Way #2 Supercomputer system at the National Supercomputer Center of Guangzhou, Guangzhou, China.

-
- * bgliu@iphy.ac.cn
- ¹ S. A. Wolf, D. D. Awschalom, R. A. Buhrman, J. M. Daughton, S. von Molnar, M. L. Roukes, A. Y. Chtchelkanova, and D. M. Treger, *Science* 294, 1488 (2001).
 - ² W. E. Pickett and J. S. Moodera, *Phys. Today* 54(5), 39 (2001).
 - ³ E. J. Jedema, A. T. Filip, and B. van Wees, *Nature* 410, 345 (2001).
 - ⁴ M. I. Katsnelson, V. Y. Irkhin, L. Chioncel, A. I. Lichtenstein, and R. A. de Groot, *Rev. Mod. Phys.* 80, 315 (2008).
 - ⁵ R. A. de Groot, F. M. Mueller, P. G. van Engen, and K. H. J. Buschow, *Phys. Rev. Lett.* 50, 2024 (1983).
 - ⁶ K. Schwarz, *J. Phys. F* 16, L211 (1986).
 - ⁷ K. P. Kamper, W. Schmitt, G. Guntherodt, R. J. Gambino, and R. Ruf, *Phys. Rev. Lett.* 59, 2788 (1987).
 - ⁸ Y. S. Dedkov, M. Fonine, C. Konig, U. Rudiger, G. Guntherodt, S. Senz, and D. Hesse, *Appl. Phys. Lett.* 80, 4181 (2002).
 - ⁹ J. Kunes, P. Novak, P. M. Oppeneer, C. Konig, M. Fraune, U. Rudiger, G. Guntherodt, and C. Ambrosch-Draxl, *Phys. Rev. B* 65, 165105 (2002).
 - ¹⁰ R. S. Keizer, S. T. B. Goennenwein, T. M. Klapwijk, G. Miao, G. Xiao, and A. Gupta, *Nature* 439, 825 (2006).
 - ¹¹ G. M. Muller, J. Walowski, M. Djordjevic, G.-X. Miao, A. Gupta, A. V. Ramos, K. Gehrke, V. Moshnyaga, K. Samwer, J. Schmalhorst et al., *Nature Mater.* 8, 56 (2009).
 - ¹² M. S. Anwar, F. Czeschka, M. Hesselberth, M. Porcu, and J. Aarts, *Phys. Rev. B* 82, 100501(R) (2010).
 - ¹³ M. S. Anwar and J. Aarts, *Phys. Rev. B* 88, 085123 (2013).
 - ¹⁴ H. Fujiwara, M. Sunagawa, K. Terashima, T. Kittaka, T. Wakita, Y. Muraoka, and T. Yokoya, *Appl. Phys. Lett.* 106, 202404 (2015);
 - ¹⁵ H. Takeda, Y. Shimizu, Y. Kobayashi, M. Itoh, T. Jinno, M. Isobe, Y. Ueda, S. Yoshida, Y. Muraoka, and T. Yokoya, *Phys. Rev. B* 93, 235129 (2016).
 - ¹⁶ A. Singh, C. Jansen, K. Lahabi, and J. Aarts, *Phys. Rev. X* 6, 041012 (2016).
 - ¹⁷ S. Sanvito and N. A. Hill, *Phys. Rev. B* 62, 15553 (2000).
 - ¹⁸ H. Akinaga, T. Manago, and M. Shirai, *Jpn. J. Appl. Phys.* 39, L1118 (2000).
 - ¹⁹ I. Galanakis, *Phys. Rev. B* 66, 012406 (2002).
 - ²⁰ B.-G. Liu, *Phys. Rev. B*, 67 (2003) 172411.
 - ²¹ W. H. Xie, Y. Q. Xu, B. G. Liu, and D. G. Pettifor, *Phys. Rev. Lett.* 91, 037204 (2003).
 - ²² S.-D. Li and B.-G. Liu, *Appl. Phys. Lett.* 104, 122408 (2014).
 - ²³ H. Kato, T. Okuda, Y. Okimoto, Y. Tomioka, K. Oikawa, T. Kamiyama and Y. Tokura, *Phys. Rev. B* 69, 184412 (2004).
 - ²⁴ Y. Kronkenberger, K. Mogare, M. Reehuis, M. Tovar, M. Jansen, G. Vaitheeswaran, V. Kanchana, F. Bultmark, A. Delin, F. Wilhelm, A. Rogalev, A. Winkler, and L. Alff, *Phys. Rev. B* 75, 020404(R) (2007).
 - ²⁵ O. N. Meetei, O. Erten, M. Randeria, N. Trivedi and P. Woodward, *Phys. Rev. Lett.* 110, 087203 (2013).
 - ²⁶ S. Gong, S.-D. Guo, P. Chen, and B.-G. Liu, *RSC Adv.* 5, 63165 (2015).
 - ²⁷ P. Blaha, K. Schwarz, P. Sorantin, and S. B. Trickey, *Comput. Phys. Commun.* 59, 399 (1990).
 - ²⁸ P. Hohenberg and W. Kohn, *Phys. Rev.* 136, B864 (1964).
 - ²⁹ W. Kohn and L. J. Sham, *Phys. Rev.* 140, A1133 (1965).
 - ³⁰ J. P. Perdew, K. Burke, and M. Ernzerhof, *Phys. Rev. Lett.* 77, 3865 (1996).
 - ³¹ F. Tran and P. Blaha, *Phys. Rev. Lett.* 102, 226401 (2009).
 - ³² D. R. Lide, *Handbook of Chemistry and Physics*, 79th ed., CRC Boca Raton, FL, 1998.
 - ³³ Y. Hinatsu, *J. Solid State Chem.* 122, 384 (1996).